



RESEARCH ARTICLE

10.1029/2017JA025082

The Association of High-Latitude Dayside Aurora With NBZ Field-Aligned Currents

J. A. Carter¹ , S. E. Milan^{1,2} , A. R. Fogg¹, L. J. Paxton³ , and B. J. Anderson³ ¹Department of Physics and Astronomy, University of Leicester, Leicester, UK, ²Birkeland Centre for Space Science, Department of Physics and Technology, University of Bergen, Bergen, Norway, ³The John Hopkins University Applied Physics Laboratory, Laurel, MD, USA

Key Points:

- High-latitude aurora and distributions of field-aligned current from both hemispheres are compared under northward IMF conditions
- These high-latitude auroras are co-located with upward NBZ field-aligned current
- The auroral emissions are only observed in the summer hemisphere, confirming a hypothesis of Frey (2007)

Correspondence to:

J. A. Carter,
jac48@leicester.ac.uk

Citation:

Carter, J. A., Milan, S. E., Fogg, A. R., Paxton, L. J., & Anderson, B. J. (2018). The association of high-latitude dayside aurora with NBZ field-aligned currents. *Journal of Geophysical Research: Space Physics*, 123, 3637–3645. <https://doi.org/10.1029/2017JA025082>

Received 6 DEC 2017

Accepted 15 APR 2018

Accepted article online 23 APR 2018

Published online 11 MAY 2018

Abstract The relationship between auroral emissions in the polar ionosphere and the large-scale flow of current within the Earth's magnetosphere has yet to be comprehensively established. Under northward interplanetary magnetic field (IMF) conditions, magnetic reconnection occurs at the high-latitude magnetopause, exciting two reverse lobe convection cells in the dayside polar ionosphere and allowing ingress of solar wind plasma to form an auroral “cusp spot” by direct impact on the atmosphere. It has been hypothesized that a second class of NBZ auroras, High-latitude Dayside Aurora, are produced by upward field-aligned currents associated with lobe convection. Here we present data from the Special Sensor Ultraviolet Spectrographic Imager instrument and from the Active Magnetosphere and Planetary Electrodynamics Response Experiment, from January 2010 to September 2013, in a large statistical study. We reveal a northward IMF auroral phenomenon that is located adjacent to the cusp spot and that is collocated with a region of upward electrical current in the clockwise-rotating lobe cell. The emission only occurs in the sunlit summer hemisphere, demonstrating the influence of the conductance of the ionosphere on current closure. In addition, fast solar wind speed is required for this emission to be bright. The results show that dayside auroral emission is produced by IMF-magnetosphere electrodynamic coupling, as well as by direct impact of the atmosphere by the solar wind, confirming the association of High-latitude Dayside Aurora with NBZ currents.

Plain Language Summary Under certain incoming solar wind conditions, patches of aurora are sometimes found not in the main bright auroral oval but inside the normally otherwise dark polar cap region. These patches of auroral emissions are collocated with regions of upward flowing electrical current. We present a study of these emissions using nearly 3 years of data from both the North and South Hemispheres, combining simultaneous observations of the polar cap at ultraviolet wavelengths, and measurements of field-aligned currents. This builds on the previous work of other authors, who observed these auroral emissions in the Northern Hemisphere only. The upward current associated auroral emissions occur when the incoming interplanetary magnetic field is northward and are shown to only be observable in the summer hemisphere. This implies a dependence on the conductance of the ionosphere, via photoionization, on the appearance of these auroras.

1. Introduction

Under northward interplanetary magnetic field (IMF, when component $B_z > 0$ nT), lobe reconnection may occur at the high-latitude magnetopause (Sandholt et al., 1998), with magnetic field lines constituting the open magnetospheric lobes. Two mechanisms have been proposed to link localized, nonfilamentary (i.e., not polar cap arcs) auroral emissions in the dayside polar cap with lobe reconnection under northward IMF. In the first, it has been shown that under northward IMF conditions, auroral emissions resulting from precipitating magnetosheath plasma, a “cusp spot,” can occur poleward of the dayside auroral oval at the footprint of this reconnection site (Frey et al., 2002; Milan et al., 2000). The cusp spot has been shown to move in response to the east-west (B_y) orientation of the IMF. For IMF $B_y \approx 0$ it is located in the noon sector, and for $B_y < 0$ nT and $B_y > 0$ nT in the Northern Hemisphere it is located in the prenoon and postnoon sector, respectively (Fuselier et al., 2003; Milan et al., 2000). The cusp spot brightness does not vary with the polarity of IMF B_y . The effect of the IMF B_y component on the high-latitude, high-altitude cusp location has also been reported via in situ measurements, for example, Escoubet et al. (2013).

©2018. The Authors.

This is an open access article under the terms of the Creative Commons Attribution License, which permits use, distribution and reproduction in any medium, provided the original work is properly cited.

The second mechanism has associated High-Latitude Detached Arcs (HiLDAs) with upward field-aligned current (FAC) produced by lobe reconnection (Frey, 2007, and references therein). Magnetic field-aligned electrical currents transmit stress from the magnetosphere to the ionosphere where they induce convective motions under the influence of solar wind-magnetosphere coupling. Under northward IMF the NBZ current system is found poleward of the main region 1-region 2 (R1-R2) system and consists of a pair of upward and downward FACs either side of the noon-midnight meridian (Iijima & Potemra, 1976a, 1976b; Iijima & Shibaji, 1987) and is associated with reverse lobe convection cells in the dayside polar cap ionosphere. For positive B_y in the Northern Hemisphere, the upward NBZ FAC expands across the noon sector, whereas for negative B_y the downward FAC will be found to enlarge. The reverse scenario occurs for currents in the Southern Hemisphere under a particular direction of B_y . Observations of the Northern Hemisphere, obtained from the Imager for Magnetopause-to-Aurora Global Exploration (IMAGE) spacecraft, identified localized HiLDA auroral features within the otherwise dark polar cap (Frey, 2007, their Figure 19, and references therein). In two HiLDA cases, the Fast Auroral SnapshoT (FAST) satellite linked these auroral features to regions of upward FAC. The authors speculated that the auroral features might be seen in the Southern Hemisphere, preferably during the summer months. A previous case study by Korth et al. (2005), taken during a 3-hr period of prolonged northward IMF, observed auroral emission coincident with NBZ FAC in the high-latitude ionosphere. Although the association between HiLDAs and FACs has been demonstrated in a limited number of cases in the Northern hemisphere (Frey et al., 2003, 2004; Korth et al., 2005), Frey (2007) called for a comprehensive statistical survey in both the Northern and Southern Hemispheres to conclusively verify this link. That is the aim of this current study.

Using auroral observations from the Defense Meteorological Satellite Program Special Sensor Ultraviolet Spectrographic Imager (SSUSI, Paxton et al., 1992) experiment, and FAC distributions constructed from the Active Magnetosphere and Planetary Electrodynamics Response Experiment (AMPERE), from the Iridium telecommunication satellite constellation (Anderson et al., 2000; Waters et al., 2001), we see a patch of auroral emission that is collocated with the upward NBZ FAC in the dayside polar cap in both the Northern and Southern Hemispheres under northward IMF conditions. The work presented here is the first comprehensive statistical study of these phenomena under varying IMF conditions, using simultaneous auroral observations from both hemispheres and with accompanying measurements of FACs for the entire period.

This paper is organized as follows. In section 2 we briefly describe our data sets and analysis methods. In section 3 we present maps of the global distributions of the FACs and compare these to auroral emissions, binned by solar wind conditions. In section 4 we discuss our results in context of two mechanisms for emission in the dayside polar cap. We conclude in section 5.

2. Data

The statistical distribution of the FACs in the Northern Hemisphere, parameterized by IMF conditions, was presented in Carter et al. (2016). Here we compare FAC distributions obtained from AMPERE to the auroral distribution constructed from data obtained by the SSUSI instrument, flown on the latest Air Force Defense Meteorological Satellite Program spacecraft (satellites F16, F17, and F18). The SSUSI scanning image spectrograph photon-counting detectors are sensitive to ultraviolet wavelengths at five spectral wavelengths or bands. Images of the auroras are built up in swaths as the satellites move along their polar Sun-synchronous orbital paths, building up a scan of the polar auroral emissions in approximately 20 min. Dayglow removal algorithms are applied to the data by the SSUSI project team (Liou et al., 2011; Paxton et al., 2017; Strickland et al., 1995, 2004; Zhang & Paxton, 2008). Dayglow is removed per pixel, maximizes at 80° solar zenith angle, and falls off smoothly and sharply with increasing solar zenith angle and along the cross-track direction from the dayside to the nightside. Dayglow is therefore not expected to introduce any strong edges or artifacts into the SSUSI images (private communication with the SSUSI instrument team). Auroral swaths are constructed for both hemispheres, with a cadence of approximately 1.5 hr. Radiance is rectified to pierce-point equivalent nadir pointing to account for slanted to vertical line of sight conversion as part of the standard SSUSI processing pipeline (Paxton & Anderson, 1992; Paxton & The SSUSI team, 2004). Here we present SSUSI radiance data in the Lyman-Birge-Hopfield long (LBHL) band (165–180 nm), and we briefly consider Lyman- α (121.6 nm) data in section 3). The SSUSI data and AMPERE data are taken during continuous and concurrent periods for both hemispheres and allow a direct comparison between FACs and auroral emissions.

Solar wind data, adjusted in time for propagation to the dayside bow shock, and from which the IMF clock angles and field magnitudes were calculated, were obtained from the OMNI database (King & Papitashvili, 2005). An additional time delay to represent the propagation of the solar wind from the bow shock to the

ionosphere was applied to the solar wind data. Following the calculations made by Jacobsen et al. (1995), we apply a total delay of 6.5 min by approximating the delay from the bow shock to the magnetopause to be 4 min, plus an additional 2.5 min to propagate from the magnetopause to the ionosphere. The data were divided into eight IMF clock angle bins, each 45° wide with the first bin centered on 0° (northward IMF), and four IMF magnitude bins (where $|B| = \sqrt{(B_Y^2 + B_Z^2)}$), from the dayside coupling parameter (Milan et al., 2012), covering 0–5, 5–10, 10–15, and 15–20 nT. Time stamps of the individual pixels of the SSUSI images were used to bin the data into average maps, in each IMF clock angle and magnitude bin.

Equivalently binned average AMPERE current density maps were taken from the work in Carter et al. (2016), although in the present study we also include data from the Southern Hemisphere. To cover the same period as our AMPERE data set, we only use SSUSI data from January 2010 to 5 September 2013.

3. Results

Average SSUSI maps in the LBHI band, using the entire data set period as described in section 2, under northward IMF conditions, and for a particular IMF magnitude bin of 5–10 nT, are plotted in Figure 1. Data are plotted using magnetic latitude and local time coordinates. Rows A and B show data from the Northern and Southern Hemispheres, respectively. Neither hemisphere data cover all local time sectors; however, the dayside polar cap is well imaged. The color scale for this figure has been saturated to highlight weaker emission features. Contours of the FAC distributions under the same IMF parameterization are plotted over the maps of Figure 1, at absolute current magnitudes of 0.1 (solid line), and 0.3 (dashed line) $\mu\text{A}/\text{m}^2$. Upward and downward directed currents are denoted by red and turquoise contours, respectively. The SSUSI spectrograph has developed a slight change in reflectivity with scan angle, possibly caused by the pyrolyzation of scan motor lubricant by solar UV radiation, that is then deposited onto the mirror (private communication with the SSUSI team). This results in a low-level residual signal on the dawnside limb that has increased during the lifetime of the satellite in orbit and is visible in Figure 1 and subsequent figures. In these images we combine data from the three spacecraft F16, F17, and F18, which were launched in different years and which therefore suffer different levels of limb degradation and independent instrumental effects. The phenomena we examine below are, however, distinguishable above any residual instrumental noise within each image.

In Figure 1 current contours (red and turquoise) for the R1–R2 system are clear and well defined as expected (Iijima & Potemra, 1976b). NBZ currents are seen inside the dayside polar cap, poleward of R1. The position of the NBZ currents within the polar cap are dependent on the B_y component (Cowley, 2000). For $B_y = 0$ the NBZ currents are symmetrical about the noon meridian, with the upward FAC in the morning sector, and the downward cell in the afternoon sector. Under positive B_y conditions in the Northern Hemisphere or under negative B_y conditions in the Southern Hemisphere, the upward cell becomes larger than the downward cell and is shifted toward noon. Conversely, under negative B_y conditions in the Northern Hemisphere or under positive B_y conditions in the Southern Hemisphere, the downward cell becomes enlarged and is shifted toward noon.

The main auroral oval is well defined for all panels of Figure 1 and is colocated with both the R1 and R2 FAC regions. There are, however, areas of additional auroral emission within the otherwise emission-free polar cap, which are associated with the upward NBZ FAC only. This emission is observed to move into the noon sector, in conjunction with the upward NBZ current, dependent on the sense of B_y orientation. This emission is most clearly seen for the Northern Hemisphere, for IMF $B_y > 0$. Panels where the downward NBZ cell dominates are devoid of NBZ-associated auroral emission. This is consistent with the appearance of the auroral emissions within the LBHI band, which are mainly driven by electron precipitation, for example, Dashkevich et al. (1993). However, other authors have noted that a substantial percentage of LBHI emission as detected by SSUSI may be driven by proton precipitation (Knight et al., 2012). We also constructed average maps at the Lyman- α band, under the same parameterizations shown in Figure 1 (not shown). No discernible emission was seen inside the structure of the main auroral oval, so we conclude that the emissions shown here, at LHBI wavelengths as detected by SSUSI, are the result of electron precipitation.

The Southern Hemisphere dayside polar cap auroral emissions are weaker than those for the north. The period of study here covers one additional Northern Hemisphere summer than Southern Hemisphere summer, which may account for a small difference in conductivity via solar ionization between the hemispheres and hence

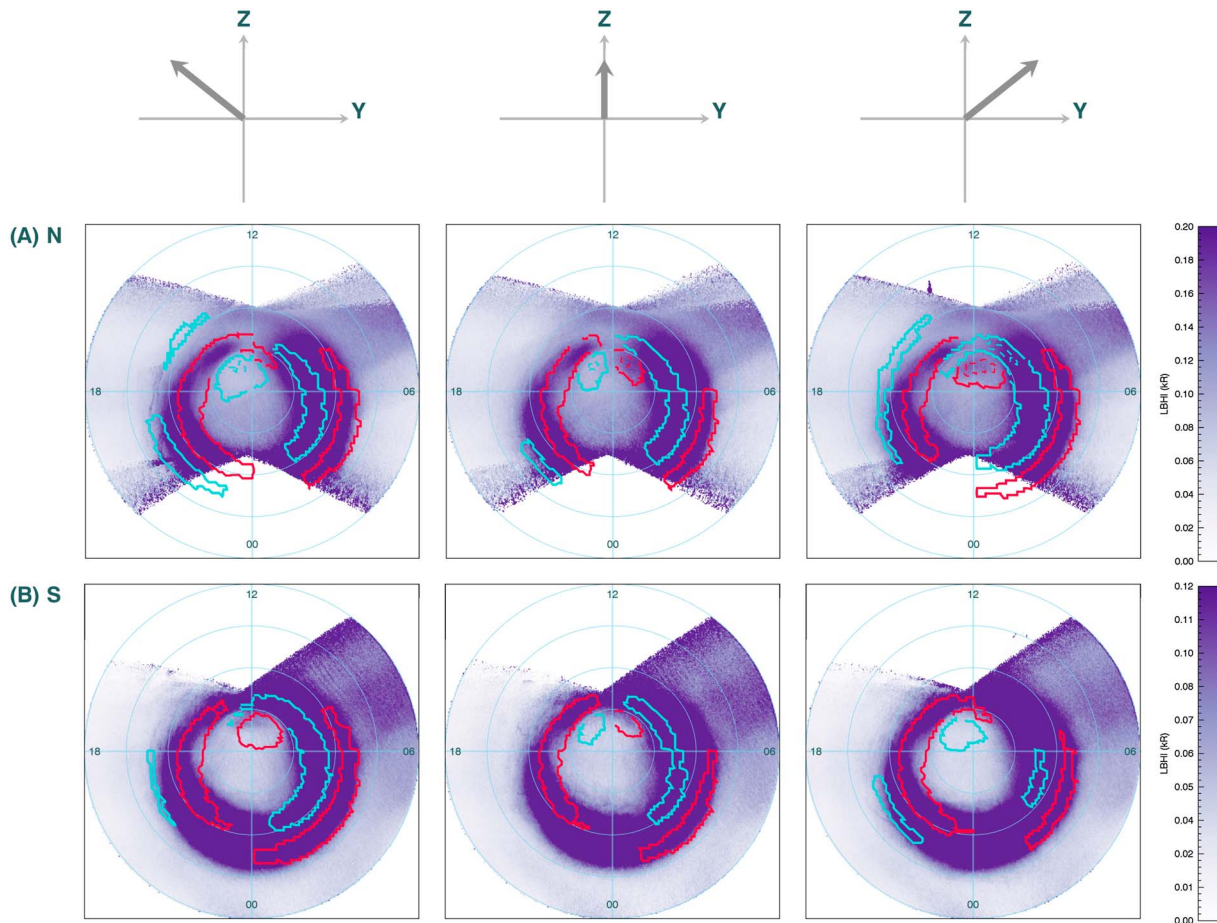


Figure 1. Auroral emissions in the Lyman-Birge-Hopfield long (LBHL) band with overlaid field-aligned current contours, for interplanetary magnetic field magnitudes 5–10 nT, under northward interplanetary magnetic field conditions in the Northern (row a) and Southern (row b) Hemispheres. Clock angles are shown above each column. Field-aligned current contours are overlaid in turquoise (downward) and red (upward) at absolute magnitudes of 0.1 (solid line), 0.3 (dashed line) $\mu\text{A}/\text{m}^2$.

slightly increased current in the Northern Hemisphere. Interhemispheric differences may be due to greater variations in the Northern Hemisphere NBZ FACs during most of the year (Coxon et al., 2016), resulting in stronger NBZ currents and therefore stronger associated auroral emissions. Upward FAC implies downward flowing electrons into the ionosphere.

When the IMF is purely northward (central panels of Figure 1, rows a and b), auroral emissions are seen collocated with the upward NBZ current in the prenoon sector of both hemispheres. In contrast, the cusp spot of previously reported IMF northward periods (Milan et al., 2000, their Figure 3, Frey et al., 2002, their Figure 12), occurred in the noon sector for the case with a near zero IMF B_y component. The auroral emissions and NBZ upward current respond in the same way to changes in the IMF B_y direction further strengthening their association.

We considered whether the upward NBZ-associated emission is controlled by the strength of various parameters of the incoming solar wind. We examined (not shown) maps for fast solar wind speed (>460 km/s), high solar wind density (>7 cm^{-3}), and high-derived solar wind pressure (>1.7 nPa), setting the thresholds at the top 20% for each OMNI parameter during our period of interest. In all cases, the auroral emissions within the polar cap remain collocated with the NBZ upward cells. NBZ-associated auroral emissions are brightest for fast solar wind speed. However, the NBZ-associated auroral emissions are less bright under the density or pressure constraints.

To test for seasonal control of the emissions via asymmetric hemispheric variations in solar illumination produced ionospheric conductivity, the data were split into summer and winter periods, approximately centered

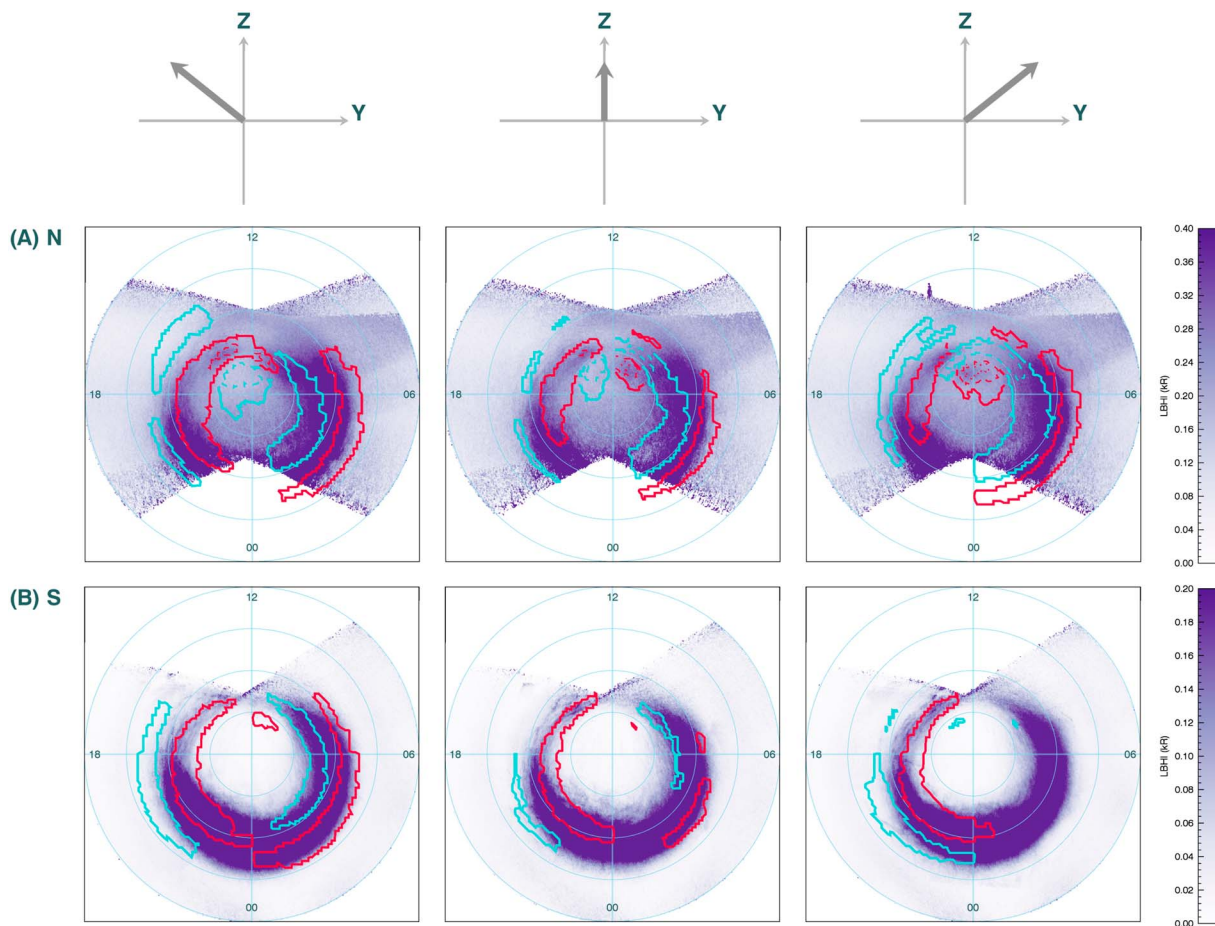


Figure 2. Season 1 (Northern Hemisphere summer) auroral emissions in the Lyman-Birge-Hopfield long (LBHI) band with overlaid field-aligned current contours, for the Northern (N, row a) and Southern (S, row b) Hemispheres. Clock angles are given in the left-hand column. Interplanetary magnetic field magnitudes are between 5 and 10 nT. Field-aligned current contours are overlaid for upward (red) and downward (turquoise) currents, at absolute magnitudes of 0.1 (solid line), 0.3 (dashed line), and 0.5 (dotted line) $\mu\text{A}/\text{m}^2$.

about the solstices. Season 1 (Northern Hemisphere summer) involved data from the months May, June, and July inclusively. Season 2 (Northern Hemisphere winter) involved data from November, December, and January. Figures 2 and 3 show northward IMF ($|B| = 5 - 10$ nT) emission maps with accompanying average FAC contours that have been seasonally selected for season 1 and season 2, respectively. FAC contours are overlaid in turquoise (downward) and red (upward) at absolute magnitudes of 0.1 (solid line), 0.3 (dashed line), and 0.5 (dotted line) $\mu\text{A}/\text{m}^2$.

For both seasons, the NBZ-associated auroral emissions are again colocated with the upward NBZ cell as it moves with the sense of IMF B_y . These NBZ-associated auroral emissions are only observed in the summer hemisphere (Figures 2a and 3b) and are absent from the winter hemisphere (Figures 2b and 3a). It is known that the magnitude of the FACs in both the main R1-R2 system and within the polar cap is dependent on solar-produced ionospheric conductance (Milan et al., 2015), and hence, a seasonal variation in this associated auroral emission is not unexpected. Previous auroral imagers have experienced considerable dayglow in the dayside polar cap, and so this NBZ-associated emission may only now be readily observable, due to improved instrumentation and dayglow removal techniques.

We also considered the standard deviation in the data, parameterized by IMF clock angle and magnitude. In Figure 4 we plot the standard deviations (row a), standard deviations divided by the mean (row b), and number of pixels that contributed to each map (row c) that applies to season 1 and the Northern Hemisphere. This figure accompanies the maps of row a of Figure 2. The standard deviation in all cases (row a) is much higher on the nightside main auroral oval compared to anywhere else in the polar cap. This is supported by the images in row b, which show that the fainter emissions, for example, equatorward of the main auroral have

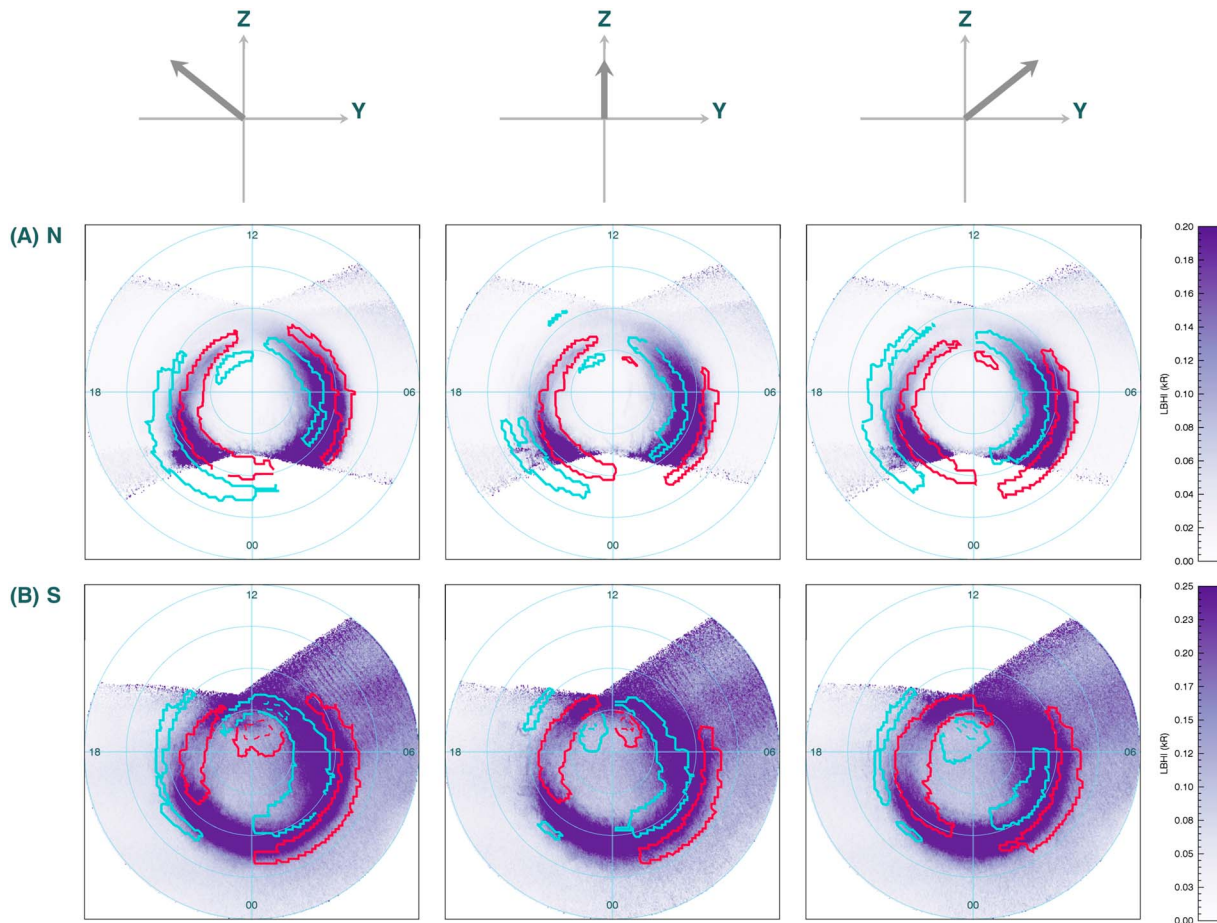


Figure 3. Season 2 (Northern Hemisphere winter) auroral emissions with field-aligned current contours, in the same format as Figure 2. LBHI = Lyman-Birge-Hopfield long.

much greater variability compared to the auroral oval and polar cap region. The central region of the maps, running approximately dusk to dawn and including where the NBZ-associated emissions occur, has been the most sampled area in all cases, as shown in row c, although the entire map is well sampled and shows little overall variation. Similar distributions in standard deviation, variability, and pixel sampling are observed for all other seasonal and hemispheric selections in this paper (not shown).

4. Discussion

This large statistical study, using data from simultaneous observations of auroral features in both hemispheres with contemporaneous measurements of field aligned currents, presents comprehensive evidence of auroral emissions associated with upward NBZ FAC in the dayside polar cap region. Using concurrent data sets we have been able to compare observations of both hemispheres as parameterized by IMF condition. The location of these emissions is robust under changing B_y orientation. These auroral emissions, also known as HiLDA (Frey, 2007), have previously been investigated but only in the Northern Hemisphere. This feature is a result of the vorticity of the reverse lobe convection cells that form in the polar cap under northward IMF conditions, and frictional coupling between the ionosphere and atmosphere, requiring upward FAC carried by downward traveling electrons. Auroral emissions are produced through the interaction of these electrons with the atmosphere, and hence, a collocation of upward FAC and polar cap auroral emissions is observed. Therefore, the location of the emission and the upward NBZ cell are inextricably linked under the influence of the IMF B_y component. This mechanism, which we discuss below, is different from the well-established mechanism producing the dayside polar cap cusp spot. The cusp spot is due to direct precipitation of magnetosheath plasma from the lobe reconnection site, and which also occurs under northward IMF conditions (Frey et al., 2003; Milan et al., 2000). A schematic of this mechanism acting in the Northern Hemisphere is presented in

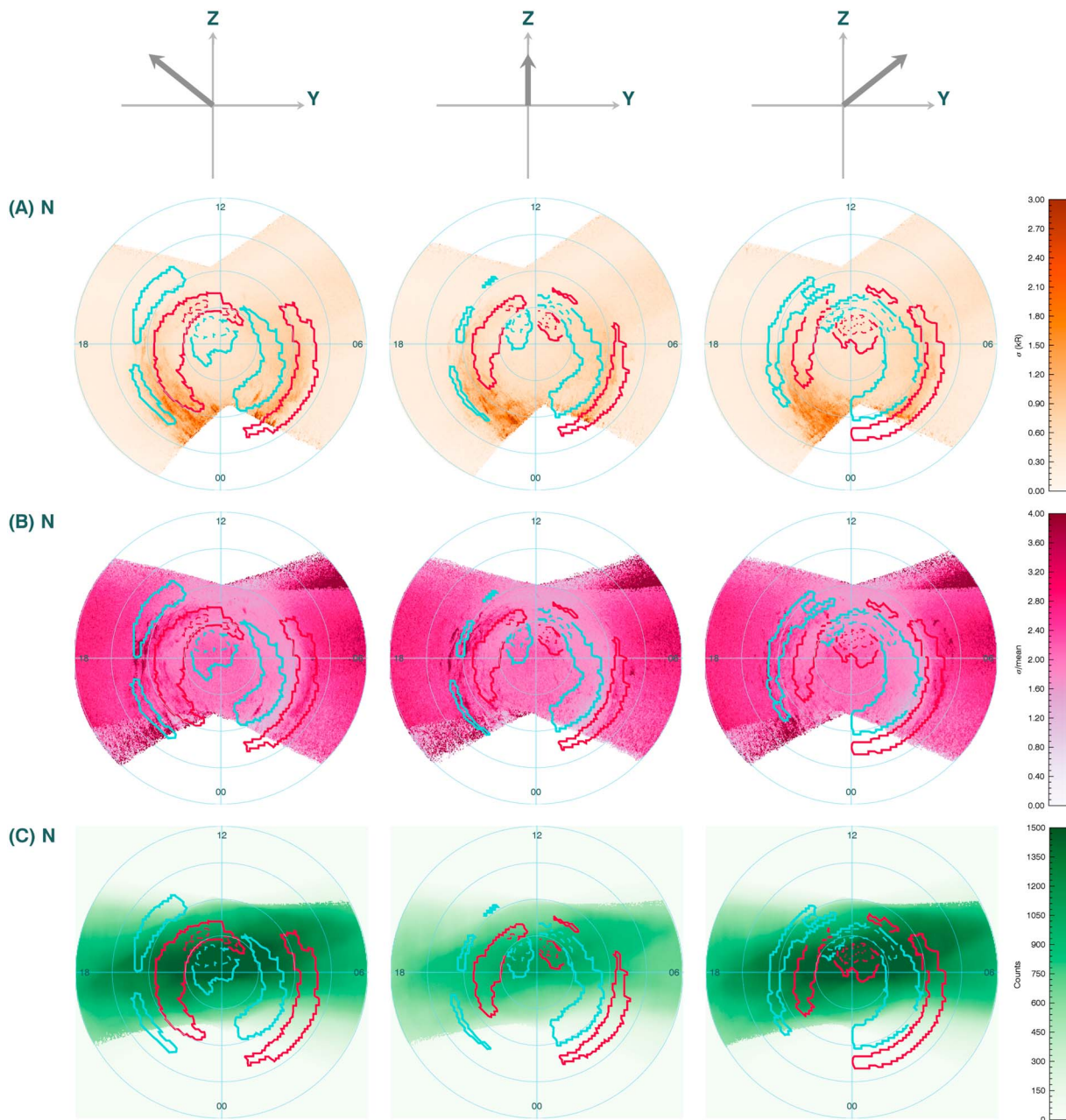


Figure 4. Season 1 (Northern Hemisphere summer) standard deviation on the average auroral emission (row a), standard deviation divided by the mean emission (row b), and pixel coverage for each map (row c), for the Northern Hemisphere. Each plot has overlaid field-aligned current contours and is in the same format as Figure 2.

Figure 5, for the IMF B_y positive and negative cases. Only the NBZ ionospheric convection cells are shown in the figure (turquoise contours), with the approximate position of the main auroral oval given for reference (green shaded area). The location of the cusp spot is also controlled by IMF B_y , as this determines where high magnetic shear is found at the high-latitude magnetopause leading to lobe reconnection (dashed gray line, Figure 5). The magnetosheath precipitation producing the cusp spot is expected to be colocated with the convection downstream of the reconnection line, forming a reversed ion dispersion signature, as reported by Woch and Lundin (1992). For a positive B_y component, this cusp spot (orange shaded areas, Figure 5b) will be found post noon, and vice versa for a negative B_y component as shown in Figure 5a (Frey et al., 2002; Fuselier et al., 2003; Milan et al., 2000). We have not been able to discern the traditional cusp spot in the result of the present statistical study, and we postulate that this is because the cusp spot is likely to occur under extreme

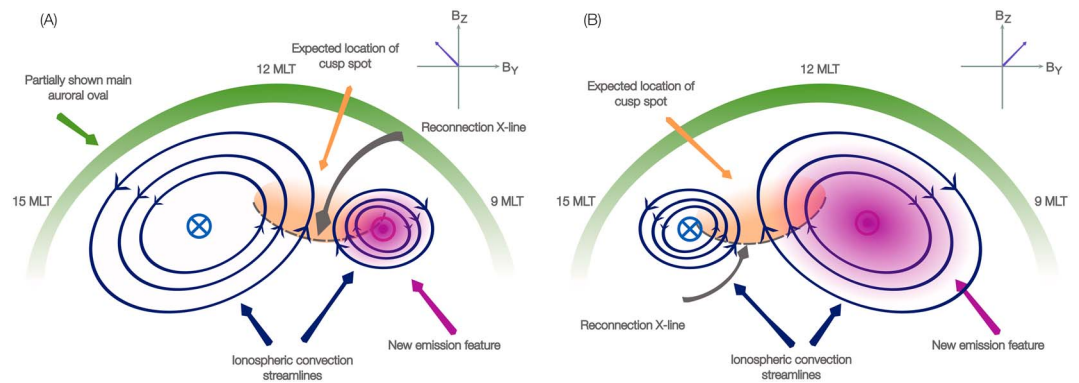


Figure 5. Schematic of the process of direct cusp spot precipitation compared to NBZ-associated auroral emissions. In (a) we plot the IMF $B_y < 0$ case, and in (b) we plot the IMF $B_y > 0$ case, both for the Northern Hemisphere dayside polar cap. Noon is toward the top of each panel. The converse situation occurs for the Southern Hemisphere for the same sense of B_y . Convection cells for NBZ (only) are shown in dark blue. The upward cell is found in the morning sector, and the downward cell is found in the afternoon sector. In each panel, cusp spot emission is shaded orange, green represents the main auroral oval, and the NBZ-associated emissions are shown in the magenta shaded areas, centered on the upward current cell.

solar wind conditions (Frey et al., 2002) not observed here. However, for the NBZ-associated emission, under $B_y = 0$ conditions the upward, clockwise NBZ cell is found in the morning sector (Cowley, 2000; Ohtani et al., 2000), growing in size and moving toward noon under positive B_y (Figure 4b) for the Northern Hemisphere, or negative B_y in the Southern Hemisphere (as postulated by Frey, 2007). The converse is true for the reverse conditions; under negative B_y in the Northern Hemisphere (Figure 5a), or positive B_y in the Southern Hemisphere, the upward FAC shrinks and is pushed up against the main auroral oval. Any NBZ-associated emissions in this case may therefore be indistinguishable from the emissions of the main auroral oval. The detectability of the auroral emissions is controlled somewhat by IMF conditions and is most evident under high solar wind speed conditions. In addition, these auroral emissions are only observable in the summer hemisphere, as suggested by Frey (2007), which is consistent with observations of NBZ currents which vanish during the equinox and winter periods (Huang et al., 2017; Stauning, 2002). This indicates a dependence on ionospheric conductivity, via photoionization in the predominantly sunlit hemisphere.

5. Conclusions

In this statistical study, we present maps of polar cap auroral emissions with accompanying FAC contours, parameterized by IMF magnitude and direction, in the LBHI band. We have shown that high-latitude dayside polar cap auroral LBHI emissions are collocated with regions of upward NBZ FAC, rather than at the ionospheric footprint of the high-latitude lobe reconnection site, known as the cusp spot. The detectability of the auroral emissions is controlled somewhat by IMF conditions and is brightest under fast solar wind speed conditions. High solar wind density is less important for the appearance of the emission. In addition, these auroral emissions are only observable in the summer hemisphere, indicating a dependence on ionospheric conductivity via photoionization in the predominantly sunlit hemisphere, confirming the hypothesis of Frey (2007).

References

- Anderson, B. J., Takahashi, K., & Toth, B. A. (2000). Sensing global Birkeland currents with iridium[®] engineering magnetometer data. *Geophysical Research Letters*, 27, 4045–4048. <https://doi.org/10.1029/2000GL000094>
- Carter, J. A., Milan, S. E., Coxon, J. C., Walach, M.-T., & Anderson, B. J. (2016). Average field-aligned current configuration parameterized by solar wind conditions. *Journal of Geophysical Research: Space Physics*, 121, 1294–1307. <https://doi.org/10.1002/2015JA021567>
- Cowley, S. W. H. (2000). Magnetosphere-ionosphere interactions: A tutorial review. In S.-I. Ohtani, et al. (Eds.), *Magnetospheric current systems*, *Geophysical Monograph Series* (Vol. 118, pp. 91). Washington, DC: American Geophysical Union. <https://doi.org/10.1029/GM118p0091>
- Coxon, J. C., Milan, S. E., Carter, J. A., Clausen, L. B. N., Anderson, B. J., & Korth, H. (2016). Seasonal and diurnal variations in AMPERE observations of the Birkeland currents compared to modeled results. *Journal of Geophysical Research: Space Physics*, 121, 4027–4040. <https://doi.org/10.1002/2015JA022050>
- Dashkevich, Z., Sergienko, T., & Ivanov, V. (1993). The Lyman-Birge-Hopfield bands in aurora. *Planetary and Space Science*, 41(1), 81–87. [https://doi.org/10.1016/0032-0633\(93\)90019-X](https://doi.org/10.1016/0032-0633(93)90019-X)
- Escoubet, C. P., Berchem, J., Trattner, K. J., Pitout, F., Richard, R., Taylor, M. G. G. T., et al. (2013). Double cusp encounter by Cluster: Double cusp or motion of the cusp? *Annales Geophysicae*, 31, 713–723. <https://doi.org/10.5194/angeo-31-713-2013>
- Frey, H. U. (2007). Localized aurora beyond the auroral oval. *Reviews of Geophysics*, 45, RG1003. <https://doi.org/10.1029/2005RG000174>

Acknowledgments

J. A. C. and S. E. M. gratefully acknowledge support from the Science Technology Facilities Council (STFC) consolidated grant ST/N000749/1. A. R. F. is supported by an STFC postgraduate studentship. The work at the Birkeland Centre for Space Science is supported by the Research Council of Norway under contract 223252/F50. The DMSP/SSUSI file type EDR-AUR data were obtained from <http://ssusi.jhuapl.edu> (data version 0106, software version 7.0.0, calibration period version E0018). AMPERE data were obtained from <http://ampere.jhuapl.edu>. Solar wind data were obtained from the NASA/GSFC OMNI facility (<http://omniweb.gsfc.nasa.gov>). The authors wish to thank the SSUSI team for providing and assisting with the data products, and to M.-T. Walach for helpful discussions. The authors extend their thanks to the anonymous referees whose comments and suggestions have greatly improved this manuscript. This research used the ALICE and SPECTRE High-Performance Computing Facility at the University of Leicester.

- Frey, H. U., Immel, T. J., Lu, G., Bonnell, J., Fuselier, S. A., Mende, S. B., et al. (2003). Properties of localized, high latitude, dayside aurora. *Journal of Geophysical Research*, *108*(A4), 8008. <https://doi.org/10.1029/2002JA009332>
- Frey, H. U., Mende, S. B., Immel, T. J., Fuselier, S. A., Claffin, E. S., Gérard, J.-C., & Hubert, B. (2002). Proton aurora in the cusp. *Journal of Geophysical Research*, *107*, 1091. <https://doi.org/10.1029/2001JA900161>
- Frey, H. U., Østgaard, N., Immel, T. J., Korth, H., & Mende, S. B. (2004). Seasonal dependence of localized, high-latitude dayside aurora (HiLDA). *Journal of Geophysical Research*, *109*, A04303. <https://doi.org/10.1029/2003JA010293>
- Fuselier, S. A., Mende, S. B., Moore, T. E., Frey, H. U., Petrinec, S. M., Claffin, E. S., & Collier, M. R. (2003). Cusp dynamics and ionospheric outflow. *Space Science Reviews*, *109*, 285–312. <https://doi.org/10.1023/B:SPAC.0000007522.71147.b3>
- Huang, T., Lühr, H., & Wang, H. (2017). Global characteristics of auroral hall currents derived from the swarm constellation: Dependences on season and IMF orientation. *Annales Geophysicae*, *35*(6), 1249–1268. <https://doi.org/10.5194/angeo-35-1249-2017>
- Iijima, T., & Potemra, T. A. (1976a). The amplitude distribution of field-aligned currents at northern high latitudes observed by Triad. *Journal of Geophysical Research*, *81*, 2165–2174. <https://doi.org/10.1029/JA081i013p02165>
- Iijima, T., & Potemra, T. A. (1976b). Field-aligned currents in the dayside cusp observed by Triad. *Journal of Geophysical Research*, *81*, 5971–5979. <https://doi.org/10.1029/JA081i034p05971>
- Iijima, T., & Shibaji, T. (1987). Global characteristics of northward IMF-associated (NBZ) field-aligned currents. *Journal of Geophysical Research*, *92*(A3), 2408–2424. <https://doi.org/10.1029/JA092iA03p02408>
- Jacobsen, B., Sandholt, P. E., Burke, W. J., Denig, W. F., & Maynard, N. C. (1995). Optical signatures of prenoon auroral precipitation: Sources and responses to solar wind variations. *Journal of Geophysical Research*, *100*(A5), 8003–8012. <https://doi.org/10.1029/94JA02726>
- King, J. H., & Papitashvili, N. E. (2005). Solar wind spatial scales in and comparisons of hourly Wind and ACE plasma and magnetic field data. *Journal of Geophysical Research*, *110*, A02104. <https://doi.org/10.1029/2004JA010649>
- Knight, H. K., Strickland, D. J., Correia, J., Hecht, J. H., & Straus, P. R. (2012). An empirical determination of proton auroral far ultraviolet emission efficiencies using a new nonclimatological proton flux extrapolation method. *Journal of Geophysical Research*, *117*, A11316. <https://doi.org/10.1029/2012JA017672>
- Korth, H., Anderson, B. J., Frey, H. U., & Waters, C. L. (2005). High-latitude electromagnetic and particle energy flux during an event with sustained strongly northward IMF. *Annales Geophysicae*, *23*, 1295–1310. <https://doi.org/10.5194/angeo-23-1295-2005>
- Liou, K., Zhang, Y.-L., Newell, P. T., Paxton, L. J., & Carbary, J. F. (2011). TIMED/GUVI observation of solar illumination effect on auroral energy deposition. *Journal of Geophysical Research*, *116*, A09305. <https://doi.org/10.1029/2010JA016402>
- Milan, S. E., Carter, J. A., Korth, H., & Anderson, B. J. (2015). Principal component analysis of Birkeland currents determined by the Active Magnetosphere and Planetary Electrodynamics Response Experiment. *Journal of Geophysical Research: Space Physics*, *120*, 10,415–10,424. <https://doi.org/10.1002/2015JA021680>
- Milan, S. E., Gosling, J. S., & Hubert, B. (2012). Relationship between interplanetary parameters and the magnetopause reconnection rate quantified from observations of the expanding polar cap. *Journal of Geophysical Research*, *117*, A03226. <https://doi.org/10.1029/2011JA017082>
- Milan, S. E., Lester, M., Cowley, S. W. H., & Brittacher, M. (2000). Dayside convection and auroral morphology during an interval of northward interplanetary magnetic field. *Annales Geophysicae*, *18*(4), 436–444. <https://doi.org/10.1007/s00585-000-0436-9>
- Ohtani, S.-I., Fujii, R., Hesse, M., & Lysak, R. L. (2000). *Magnetospheric current systems*, *Geophysical Monograph Series*. Washington, DC: American Geophysical Union.
- Paxton, L. J., & Anderson, D. E. (1992). Far ultraviolet remote sensing of Venus and Mars, *Venus and Mars: Atmospheres, ionospheres, and solar wind interactions*, *Geophysical Monograph Series* (Vol. 66, pp. 113–189). Washington, DC: American Geophysical Union. <https://doi.org/10.1029/GM066p0113>
- Paxton, L. J., Meng, C.-I., Fountain, G. H., Ogorzalek, B. S., Darlington, E. H., Gary, S. A., et al. (1992). Special Sensor Ultraviolet Spectrographic Imager (SSUSI)—An instrument description. In *Instrumentation for Planetary and Terrestrial Atmospheric Remote Sensing: Proceedings of the Meeting* (pp. 2–15). San Diego, CA. <https://doi.org/10.1117/12.60595>
- Paxton, L. J., Schaefer, R. K., Zhang, Y., & Kil, H. (2017). Far ultraviolet instrument technology. *Journal of Geophysical Research: Space Physics*, *122*, 2706–2733. <https://doi.org/10.1002/2016JA023578>
- Paxton, L. J., & The SSUSI team (2004). Algorithm theoretical basis document for environmental data records from the Space Environmental Sensor Suite, John Hopkins Applied Physics Laboratory.
- Sandholt, P. E., Farrugia, C. J., Moen, J., Norberg, Ø., Lybekk, B., Sten, T., & Hansen, T. (1998). A classification of dayside auroral forms and activities as a function of interplanetary magnetic field orientation. *Journal of Geophysical Research*, *103*(A10), 23,325–23,345. <https://doi.org/10.1029/98JA02156>
- Stauning, P. (2002). Field-aligned ionospheric current systems observed from Magsat and Oersted satellites during northward IMF. *Geophysical Research Letters*, *29*(15), 8005. <https://doi.org/10.1029/2001GL013961>
- Strickland, D. J., Evans, J. S., & Paxton, L. J. (1995). Satellite remote sensing of thermospheric O/N₂ and solar EUV: 1. Theory. *Journal of Geophysical Research*, *100*, 12,217–12,226. <https://doi.org/10.1029/95JA00574>
- Strickland, D. J., Lean, J. L., Meier, R. R., Christensen, A. B., Paxton, L. J., Morrison, D., et al. (2004). Solar EUV irradiance variability derived from terrestrial far ultraviolet dayglow observations. *Geophysical Research Letters*, *31*, L03801. <https://doi.org/10.1029/2003GL018415>
- Waters, C. L., Anderson, B. J., & Liou, K. (2001). Estimation of global field aligned currents using the iridium[®] system magnetometer data. *Geophysical Research Letters*, *28*, 2165–2168. <https://doi.org/10.1029/2000GL012725>
- Woch, J., & Lundin, R. (1992). Magnetosheath plasma precipitation in the polar cusp and its control by the interplanetary magnetic field. *Journal of Geophysical Research*, *97*, 1421–1430. <https://doi.org/10.1029/91JA02487>
- Zhang, Y., & Paxton, L. J. (2008). An empirical K_p-dependent global auroral model based on TIMED/GUVI FUV data. *Journal of Atmospheric and Solar-Terrestrial Physics*, *70*, 1231–1242. <https://doi.org/10.1016/j.jastp.2008.03.008>